Designed Isomorphism of Nifedipine: A Joint Experimental and Molecular Simulation Study with Screened Solvents and Antisolvents

ARTICLE *in* CRYSTAL GROWTH & DESIGN · DECEMBER 2013

Impact Factor: 4.89 · DOI: 10.1021/cg401612z

CRYSTAL GROWTH & DESIGN

Article

pubs.acs.org/crystal

Designed Isomorphism of Nifedipine: A Joint Experimental and Molecular Simulation Study with Screened Solvents and Antisolvents

Dinesh Kumar and Nalini R Shastri*

National Institute of Pharmaceutical Education & Research, Hyderabad 500 037, India

Supporting Information

ABSTRACT: Controlling the shape of crystals is of great practical relevance in pharmaceutical manufacturing. In the present study, an attempt was made to correlate experimental and simulated crystal habits of nifedipine (Nif). Modified habits with isodiametric morphology were observed in the following solvent and solvent/antisolvent pairs; chloroform/hexane, chloroform/isopropyl alcohol (IPA), dichloromethane (DCM), DCM/IPA, and ethanol/hexane. Presence of any solvates or polymorphs was ruled out by using differential scanning calorimetry, thermogravimetric analysis, Fourier transform infrared spectroscopy, and powder X-ray diffraction. A solvent effect was introduced by surface docking to bridge the gap between experimental and simulated habits as they deviated from vacuum morphology. Molecular dynamics was performed, and modified attachment energy was calculated to obtain the final morphology. The achieved predictions were found to be in good agreement with the experimental habits (statistically significant with $p < 0.05$). Similarly, significant enhancement (1.5−2.5 times) in solubility and dissolution behavior of the modified habits was observed compared with the untreated drug. Nif with chloroform/IPA combination showed isodiametric habit with better solubility and dissolution rate, which was attributed to their high surface/volume ratio. Good correlation was observed between polarity of crystallization solvents and nature of functional moiety of a specific facet. The methodology used here could prove to be a powerful tool for selection of habit modifying solvents since prediction of morphologies was demonstrated successfully.

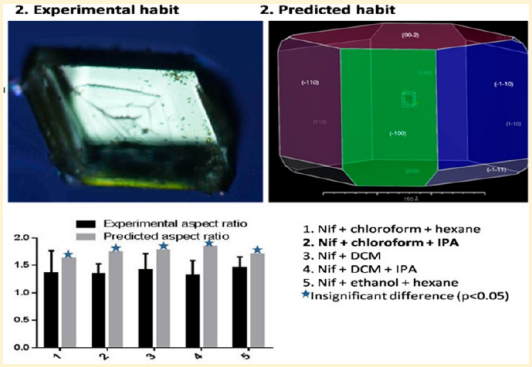

1. INTRODUCTION

The majority of the pharmaceutical materials exist in solid crystalline forms with a tendency to exhibit polymorphism or isomorphism.[1] Polymorphism is described as an ability of a substance to exist in alternate crystalline phases having different arrangements or conformations of molecules in the crystal lattice, whereas overall crystal shape is described as morphology (in vacuo) or habit (experimental).[2−4] Crystal habit or isomorphs may or may not be altered with polymorphic transformation.[5] The various known crystal habits includes cubic, needle, lath, plate, tabular, etc. Although isotropic crystals (cubic, spherical) are considered as preferred habits, a majority of drugs exist as nonisotropic crystals (needle, plate, etc.).[6] Crystal habit of a drug is an important variable in pharmaceutical manufacturing. A number of basic physicochemical properties such as solubility and dissolution rate[7] and certain micromeritic properties like tablet compressibility, mechanical strength, and powder flow[4,8] depend on and vary according to their habit.[9,10] It has been previously reported that solvents of different polarity used during the crystallization of chemical compounds can influence the morphology.[11] In many reported case studies, crystal engineering strategies have been used to generate crystals of the desired architecture with some degree of success.[12−14] The importance of crystal habit on product development is currently geared toward simulating the solid-state properties using molecular modeling with prediction approaches.[15,16] A combined modeling and experimental strategy can hence be used for obtaining crystals of desired architecture.[1,17]

Nifedipine (Nif), a potent calcium channel blocker, was chosen as a model drug for this study. It is widely used as an antianginal and an antihypertensive drug.[18] However, the therapeutic efficacy of Nif has been limited by its poor intrinsic water solubility of 5−6 μg/mL over a pH range of 4−13 (practically insoluble).[19] Polymorphic behavior of Nif is still unclear. Nif is mostly reported in the thermodynamically most stable α form (monoclinic); however a few authors have also reported the presence of two other polymorphs named β (triclinic) and γ, which they generated after quench cooling of melted Nif.[20−22] Various formulation approaches for dissolution rate enhancement of Nif have been reported with mixed results, which include hydroxy-propyl methylcellulose compacts, formation of solid dispersions, inclusion complexes, and nanocrystals.[23] These novel formulations have shown significant improvement in solubility and bioavailability. In comparison to the above-mentioned techniques, crystal habit

Received: October 29, 2013
Revised: November 18, 2013
Published: November 22, 2013

modification is a cheaper and widely established technique for improving solubility and dissolution.[12] Thus, Nif was selected as model drug due to its poor pharmaceutical and biopharmaceutical availability.

Various eminent scientists have tried systemic crystal habit modification of various drugs with the help of simulation studies, which helps in understanding the possible mechanism of interaction between crystal faces and crystal habit modifiers which can be solvent, antisolvent, or any other additive.[14,24−26] The objective of this work was to systematically modify the crystal habit of Nif and carry out simulation studies with crystallization solvents. Five crystal habits of Nif were obtained by controlled crystallization. BFDH (Bravais−Friedel−Donnay−Harker), surface free-energy, and attachment energy models were applied to obtain preliminary simulation results. The attachment energy calculations predicted a growth morphology in vacuum that was dominated by (100), (011), (110), (002), (11$\bar{1}$), and (10$\bar{2}$) facets. However, due to the notable difference between simulation and experimental results, a solvation effect was employed by introducing an interface layer model to simulate crystallization environment. Based on molecular dynamics (MD) simulation, the final crystal habits derived from the interface layer model were highly in accord with the recrystallized crystal habits. MD simulations were implemented to study the effect of various polar and nonpolar solvents on different faces of the Nif crystals. The surface functionalities of a particular crystal face were correlated with molecular functionalities of crystallization solvents. Results from FTIR (Fourier transform infrared), p-XRD (powder X-ray diffraction), DSC (differential scanning calorimetry) and TGA (thermogravimetric analysis) led to the conclusion that only habit modifications were observed during recrystallization. Selected crystals showed significant improvement in equilibrium solubility and dissolution rate, which correlated well with their respective simulated surface/volume ratio.

2. EXPERIMENTAL SECTION

2.1. Materials. Nif was received as a gratis sample from Mylan Laboratories (Hyderabad, India). Tween 20 was purchased from SD Fine chemicals Ltd., India. Acetonitrile (HPLC grade) was purchased from Ranchem Fine Chemicals, India. In-house ultrapure water from Millipore was used for all the experiments. All other chemicals used were of analytical grade. Amber colored glassware was used for all experiments and storage. All experiments were conducted in dark conditions.

2.2. High-Performance Liquid Chromatography (HPLC). All the samples were analyzed for drug content using a previously reported HPLC method with slight modifications.[27] The HPLC system (LC-20 AD, Shimadzu, Japan) consisted of an HPLC pump and manual injector equipped with a UV detector (SPD-20A). Methanol/water was used as mobile phase in 60:40 (v/v) ratios with flow rate of 1 mL/min. A 20 μL sample was injected, and absorbance was recorded at 238 nm.

2.3. Solubility Studies. Solvents were selected in increasing order of polarity and dielectric constants (Table 1). Solubility studies were performed using the selected solvents to determine the saturation solubility. Solubility of plain Nif in different solvents was determined by placing an excess amount of drug with 10 mL of solvent in screw capped glass vials. These vials were then stirred mechanically in a shaker at a constant temperature of 37 °C with a speed of 100 rpm. Samples were withdrawn after 72 h, filtered using 0.2 μm membrane filters, and then analyzed after appropriate dilution in methanol using HPLC. Equilibrium solubility was also determined for selected crystal habits of Nif in 0.05% Tween 20 in distilled water.[28] An accurately weighed amount (20 mg) of drug sample (n = 3) having different crystal habit was added to the selected solubility medium. Samples were withdrawn at 72 h, filtered, and analyzed for drug concentration by HPLC.

Table 1. Nif Recrystallization with Screened Solvents and Solvent−Antisolvent Combinations

antisolvent	solvent	solubility (mg/mL)	crystal habit	average aspect ratio[a] ± SD
without antisolvent	chloroform	130	platy	2.864 ± 0.540
	ethyl acetate	50	platy	2.347 ± 0.850
	DCM	160	nearly spherical	1.320 ± 0.264
	acetone	240	rod	1.545 ± 0.446
	ethanol	17	no regular crystal obtained	*b*
	methanol	26	no regular crystal obtained	*b*
hexane	chloroform		nearly cubical	1.357 ± 0.406
	ethyl acetate		platy	2.619 ± 0.780
	DCM		platy	2.009 ± 0.043
	ethanol		∼spherical	1.459 ± 0.194
	methanol		platy	1.688 ± 0.437
	acetonitrile		tabular	2.841 ± 0.327
IPA	chlororform		cubical with platy	1.338 ± 0.188
	ethyl acetate		tabular	1.721 ± 0.044
	DCM		nearly cubical	1.410 ± 0.300
	ethanol		platy	1.967 ± 0.327
	acetonitrile		tabular	2.192 ± 0.130

[a]All values are expressed as mean ± SD (n = 50). [b]Not determined.

2.4. Recrystallization Experiments. A crystallization protocol, encompassing process variables such as polarity, dielectric constants, crystallization time, and temperature, was developed. Based on Nif solubility data, solvents were classified as good solvents and antisolvents. The solvents were maintained at their boiling temperature. A slight excess amount of Nif (as determined by solubility studies) was dissolved in 4 mL of solvent. For crystallization with solvent/antisolvent combinations, a slight excess of Nif was dissolved in 3 mL of solvent followed by 1 mL of antisolvent addition. The solution was filtered into a crystallization vessel and allowed to cool for supersaturation. The evaporation rate was controlled using an inverted funnel. After 24 h, crystals were collected, dried, weighed, and stored in amber colored bottles. These crystals were then used for further characterization.

2.5. Characterization of Crystallized Solid Forms. *2.5.1. Microscopy.* Crystal habits were observed at different magnifications by inverted polarized microscope (Nikone TiU) operating with NIE software. A cross-polarizer was used for observing the birefringence. Aspect ratios and particle sizes were also determined.

2.5.2. Differential Scanning Calorimetry (DSC). Conventional DSC analysis was conducted to determine melting point and enthalpy values using a Mettler Toledo DSC system operating with Star software. Indium was used for calibration. The sample cell was purged with dry nitrogen at a flow rate of 60 mL/min. Accurately weighed samples (3−10 mg) in aluminum crimped pans were scanned at a heating rate of 10 °C/min over a temperature range of 25−220 °C.

2.5.3. Thermogravimetric Analysis (TGA). Presence of solvent or any degradation during heating was examined using TGA (ExStar TGA/DTA 7200) operating with Muse software. Accurately weighed (5−10 mg) samples were loaded in alumina crucibles and heated at a rate of 20 °C/min over a temperature range of 25 to 400 °C under a nitrogen purge of 60 mL/min.

2.5.4. Fourier Transform Infrared (FTIR) Spectroscopy. Samples of about 5 mg were mixed thoroughly with 100 mg of potassium bromide IR powder and compacted under vacuum at a pressure of 12 psi for 3 min. The resultant disk was mounted in a suitable holder in a

dx.doi.org/10.1021/cg401612z | Cryst. Growth Des. 2014, 14, 326−338

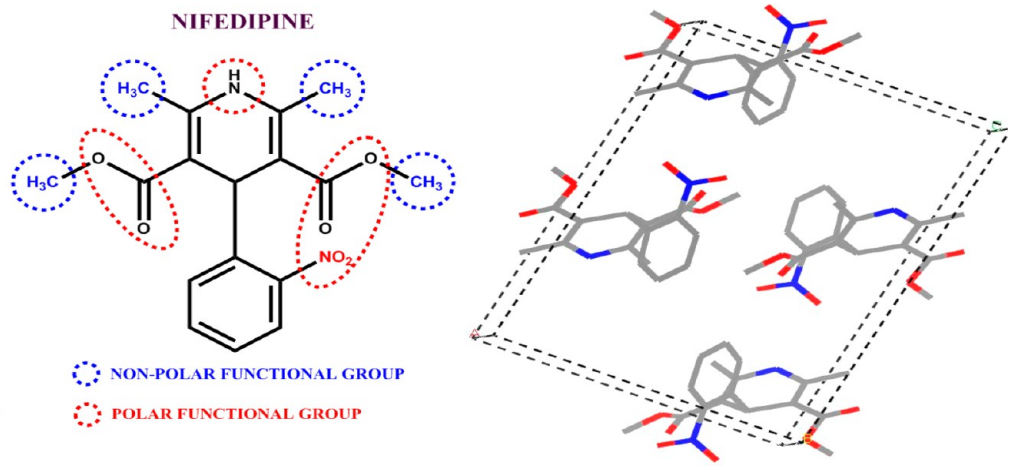

Figure 1. Molecular structure and crystal structure of Nif obtained from Cambridge Crystal Structure Database (CCSD).

PerkinElmer IR spectrophotometer, and the FTIR spectrum was recorded from 4000 to 625 cm^{-1} in a scan time of 12 min.

2.5.5. Powder X-ray Diffraction (PXRD). PXRD patterns of samples were recorded at room temperature on an X-ray powder diffractometer (X′Pert Pro PANalytical), using Ni-filtered Cu Kα radiation (wavelength = 1.5406 Å). The data were recorded over a scanning 2θ range of 2° to 50° at step time of 0.045 steps/0.5 s.

2.5.6. In Vitro Dissolution Studies. Dissolution experiments of different crystal habits in triplicate were carried out in a USP Apparatus II (paddle-type) with rotational speed of 50 rpm. Accurate amounts of samples (dose equivalent to 20 mg) were added to dissolution medium (0.05% Tween 20 in distilled water).[28] Samples were withdrawn at appropriate intervals though a syringe attached to a membrane filter (0.45 μm). An equal volume of fresh dissolution medium was replaced. The samples were analyzed for drug concentration using HPLC.

2.6. Computer Simulation Details and Theory. The crystal structure of Nif (ref code BICCIZ) was taken from CSD (Cambridge Structural Database). Crystal dimensions were defined in terms of length, height, and width as *a*, *b*, and *c* and angles between them as α, β, and γ. Nif monoclinic P_1 crystal cell parameters are as follows: *a* 10.92 Å, *b* 10.32 Å, *c* 14.81 Å, α 90°, β 92.7°, and γ 90° (Figure 1). All MD and morphology predictions were performed using Materials Studio 6.1 software program, Materials Studio 6.1 (Accelrys Inc., USA) with the COMPASS (condensed phase optimized molecular potentials for atomistic simulation studies) force field. Geometry optimization was done with the forcite algorithm with COMPASS force field. The face list was generated using morphology calculation, which gave *hkl* values of important faces with d_{hkl} values. The general procedure of modeling the modified crystal morphology was developed on the basis of the reported literature.[29]

2.6.1. Conventional Morphology Prediction Models (in Vacuum). The first theoretical model used was BFDH, which generated a list of possible growth faces and their relative growth rates.[3,25] The method is an approximation and does not account for the energetics of the system.[30] The stronger the bonding effects in the crystal, the less accurate is the method.[31] In many cases, however, good approximations can be obtained, and the method is thus useful for identifying important faces in the growth process.[31,32] The second model used was the attachment energy model, which is also called the growth morphology method. The growth morphology method assumes that the growth rate of a crystal face is proportional to its attachment energy, that is, faces with the lowest attachment energies are the slowest growing and, therefore, have the most morphological importance.[30,31,33] The attachment energy was calculated for a series of suitable slices (*hkl*) that were chosen by performing a Donnay−Harker prediction. From the energy calculation, and hence the growth rate, a center-to-plane distance was assigned to each face. This information was used to deduce the morphology. The third prediction model used was the surface free energy model, which is also called the equilibrium morphology method. The equilibrium morphology method calculated the surface energy at a temperature of 0 K.[30] This method determined the equilibrium morphology of a crystal by calculating the minimum of the surface free energy for a given volume and temperature.[31,32]

2.6.2. Surface Docking Approach. The surface docking approach is a prediction approach developed to simulate the influence of additives on the crystal morphology.[34] If the additive has a strong interaction on one specific face, the growth rate of this face will be slowed, and this face will become larger compared with the other faces thus guiding the final morphology.[31] Molecular mechanics potential-energy minimization was performed on the unit cell, and cell parameters were optimized by smart minimizer. For the solid side consideration, the pure crystal morphology was calculated using attachment energy method and faces with morphology importance (MI) were determined.[29] The attachment energy model generated a list of possible crystal faces in which the morphology was dominated by (100), (011), (110), (002), (11$\bar{1}$), (111), (10$\bar{2}$) and (012) crystal facets. These eight faces of the highest morphological importance were selected and supplied with the required lattice parameters for the amorphous cell.[30] The Nif crystal was cleaved parallel to the (*hkl*) plane with a depth of four unit cell. A crystal slice was constructed as a periodic superstructure of 3 × 2 unit cells. Subsequently, the crystal slice was optimized by the molecular mechanics and MD.[31] A solvent layer containing 100 molecules was constructed by the Amorphous Cell tool and refined by MD techniques. The dimensions of the amorphous cell were predetermined by the lattice parameters of the selected crystal surface.[31] The next task involved optimization of the amorphous cell. All amorphous cells were minimized at 10 000 iteration steps. Energy minimization was implemented with the Newton method. The subsequent equilibration on the cell comprised 100 ps *NVE* (*N* = constant number of particles, *V* = constant volume, *E* = constant energy) and 5 ps Parrinello−Rahman, *NPT* (*P* = constant pressure, *T* = constant temperature) runs.

A two-layer interfacial model was employed for MD simulation to study the influence of the solvent on the crystal shape.[31] One part of the model was the crystal slice, and another was occupied by the solvent layer. The concentration of solvent molecules was based on the experimental solubility data. The final simulation model consists of 24 Nif molecules and 100 solvent molecules (75 solvent molecules and 25 antisolvent molecules in combination study). Constraints were fixed for the whole crystal slice. A near 10 Å thickness vacuum slab was built above the solvent layer. The energy minimization for the interfacial model was carried out before the dynamics simulation. For the modeling of the combined solid and liquid system, each of the equilibrated cells was attached to the associated surface. In this context, the amorphous cell was named "amorphous layer". *NVT* calculations on this layered setup were conducted for 10 ps at a time step of 1 fs. The *NVT* simulations were performed with the Nose Scale

dx.doi.org/10.1021/cg401612z | *Cryst. Growth Des.* 2014, 14, 326−338

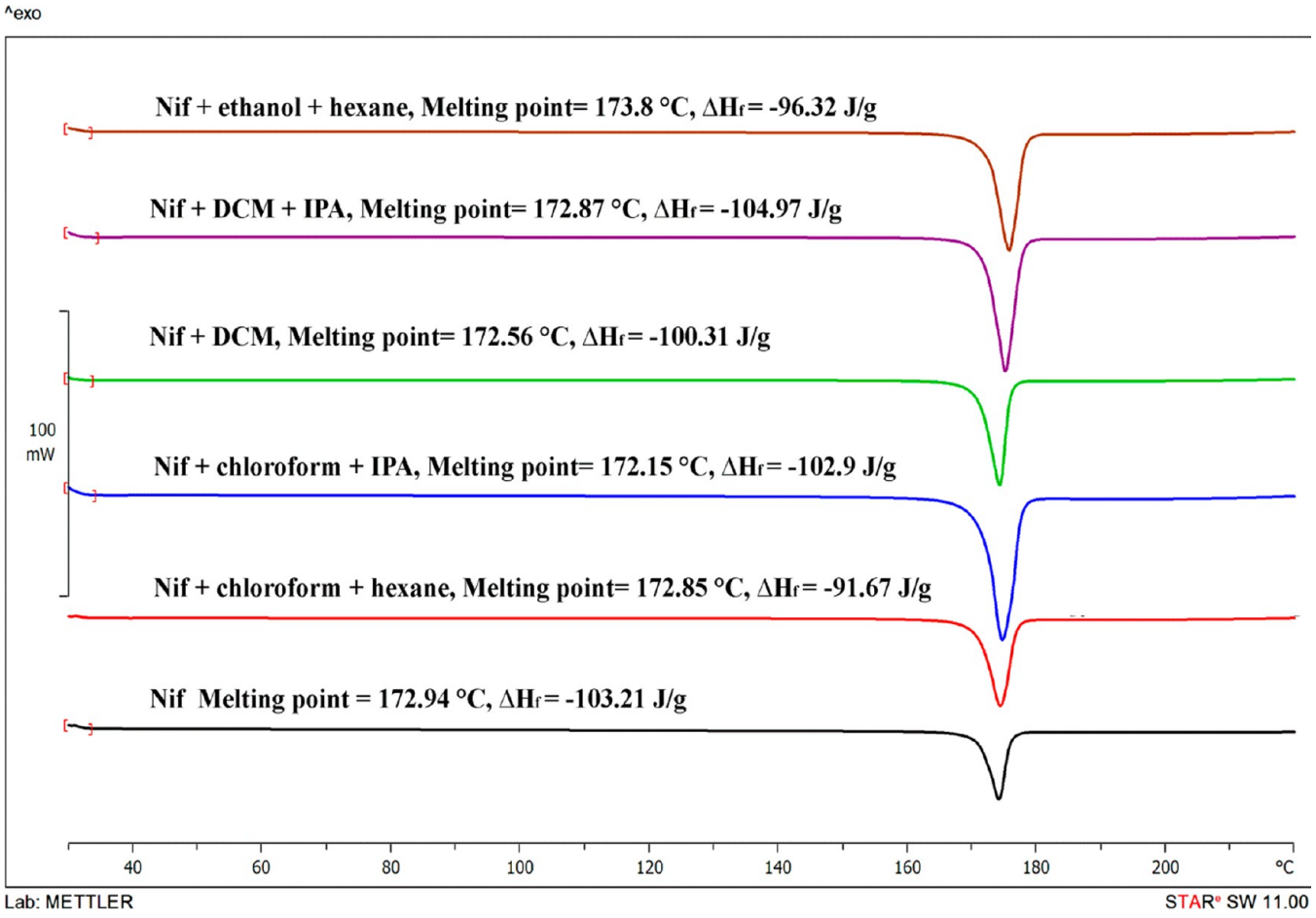

Figure 2. DSC thermographs of various selected formulations.

algorithms of temperature control. The minimum energy conformation of the system was minimized for further 10 000 iterations. The obtained potential energy of the structure containing both crystal surface and amorphous layer was denoted as E_{total}. Subsequently the energies of the separated structures of the surface and the amorphous layer were calculated and denoted as $E_{surface}$ and $E_{amorphous}$, respectively.

2.6.3. Generation of Modified Morphology from Modified Attachment Energy. For the equilibration stage, the time step for the MD simulation was fixed with defined period (10 ps). After equilibrating the system, the production stage was performed. The Coulombic and van der Waals interactions were calculated by employing the standard Ewald summation method to determine the potential-energy calculations. Modified attachment energy (MAE) was then calculated by the formula[14,33,35,36]

$$^{mod}E_{att} = E_{total} - (E_{surface} + E_{amorphous})$$

where $^{mod}E_{att}$ represents the modified attachment energy of a selected solvent with a specific crystal face and E_{total} represents the minimized energy of the layer. $E_{surface}$ represents the energy of the sliced crystal surface from the layer, and $E_{amorphous}$ represents the energy of the sliced solvent surface from the layer. The modified habit was generated based on the relation stated by Hartman and Bennema.[36]

$$R_g \approx [^{mod}E_{att}]$$

where R_g represents the growth rate in a particular direction, which is directly proportional to the modified attached energy. The morphology tool of Material Studio 6.1 was employed for the prediction of the morphology in the presence of the given solvent.

3. RESULTS AND DISCUSSION

3.1. Solubility Studies. As shown in Table 1, Nif shows good solubility in chloroform, ethyl acetate, DCM, ethanol, and methanol, whereas it was found to be poorly soluble in hexane and IPA.

3.2. Crystallization Experiments. *3.2.1. Recrystallization from Different Solvents.* Habits were modified successfully with chloroform, ethyl acetate, DCM, and acetone, whereas with other solvents no regular crystals were obtained (Table 1). Nearly spherical/isodiametric crystals were obtained with DCM and were selected for further studies due to their lower aspect ratios. Ethanol and methanol were not selected because of the absence of organized crystal shape, whereas chloroform, ethyl acetate, and acetone were not selected due to the higher aspect ratio crystals obtained.

3.2.2. Crystallization by the Antisolvent Technique. Nearly isodiametric crystals were obtained with the combination of chloroform and hexane (cubical), ethanol and hexane (~cubical), chloroform and IPA (cubical with platy), and DCM and IPA (~cubical). The solvent/antisolvent combinations that gave crystals with aspect ratio of nearly 1 were selected for further studies (Table 1). Other combinations were not selected because of the higher aspect ratio crystals produced.

3.3. DSC and TGA of Selected Crystals. DSC data for untreated and treated Nif crystals are shown in Figure 2. The DSC thermograms of all treated samples were identical to that of untreated Nif. The DSC curve of untreated Nif showed a

dx.doi.org/10.1021/cg401612z | Cryst. Growth Des. 2014, 14, 326−338

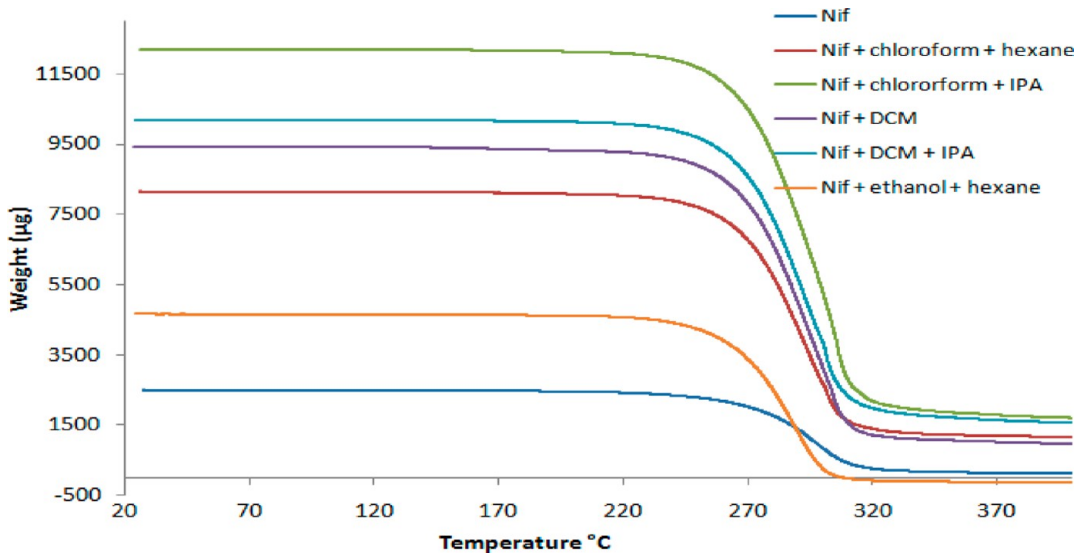

Figure 3. TGA thermographs of various selected formulations.

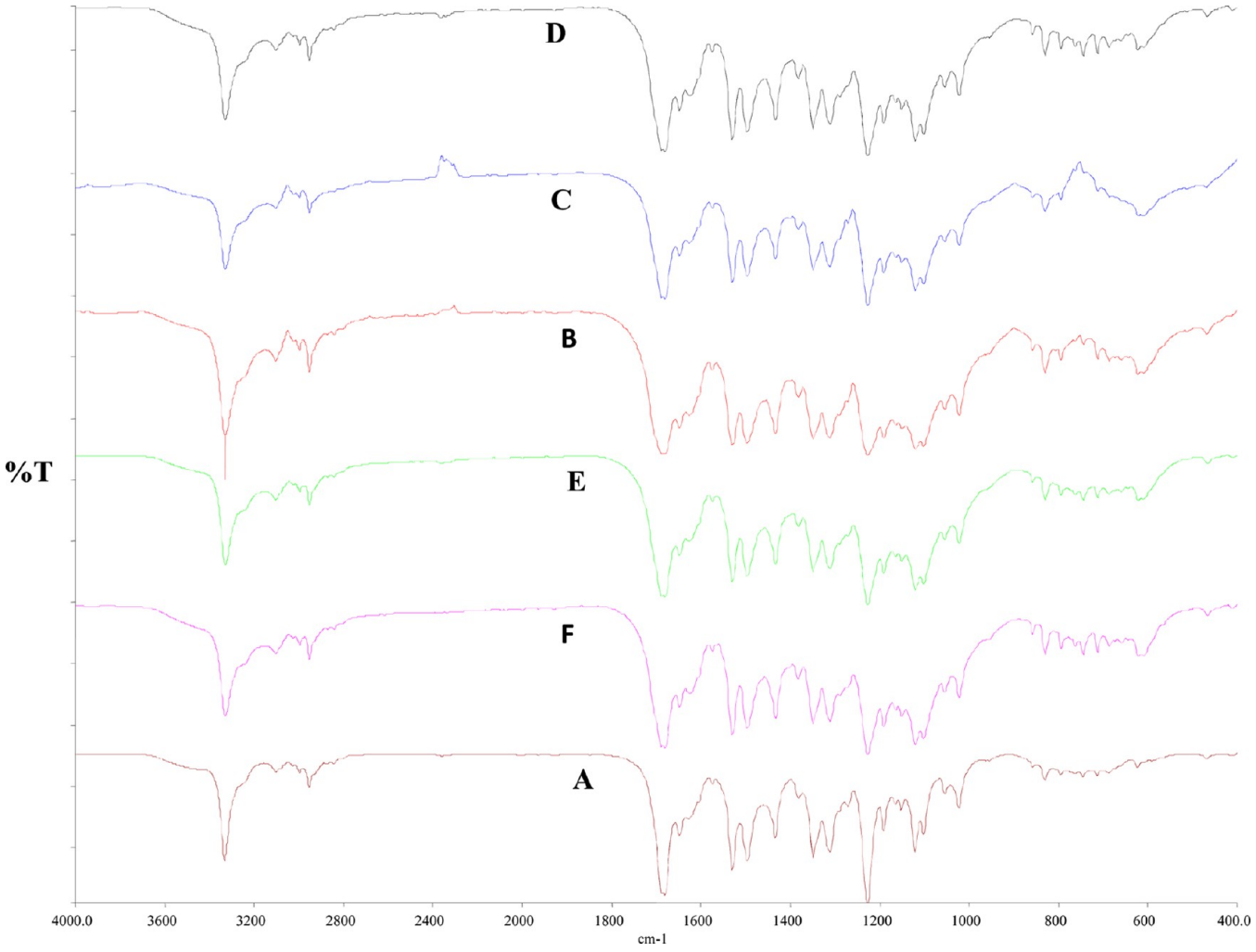

Figure 4. FTIR of selected Nif formulations: (A) untreated Nif; (B) Nif in chloroform/hexane; (C) Nif in chloroform/IPA; (D) Nif in DCM; (E) Nif in DCM/IPA; (F) Nif in ethanol/hexane.

sharp single endothermic peak at 172.94 °C corresponding to the melting point of Nif. Similarly, all recrystallized samples in different solvents also showed a single melting point endotherm in the range of 172.12−173.8 °C. The small shift in the melting point could be attributed to the difference in the crystal size since the samples were not crushed to uniform sized particles

dx.doi.org/10.1021/cg401612z | *Cryst. Growth Des.* 2014, 14, 326−338

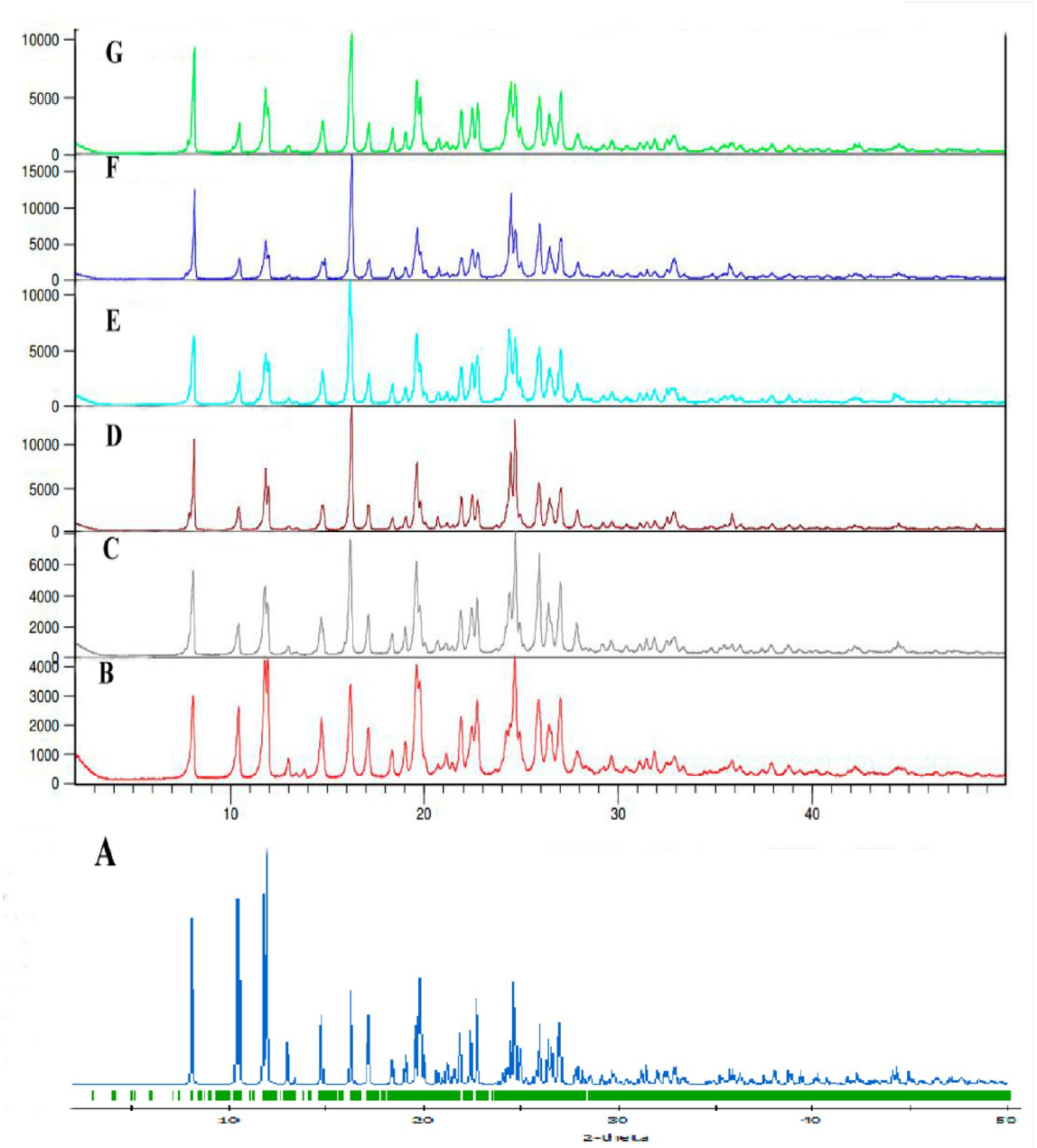

Figure 5. p-XRD results of selected Nif formulations: (A) simulated p-XRD of Nif; (B) untreated Nif; (C) Nif in chloroform/hexane; (D) Nif in chloroform/IPA; (E) Nif in DCM; (F) Nif in DCM/IPA; (G) Nif in ethanol/hexane.

before being subjected to DSC, in order to avoid grinding-induced solid state transitions. Nifedipine has been reported to exist in three monotropically related polymorphic forms, form α (melting point ~173 °C), form β (melting point ~163 °C), and form γ (melting point ~135 °C).[37,38] Form α is reported as thermodynamically stable at room temperature, whereas forms β and γ, which are metastable modifications, can be obtained only from supercooled melt of Nif.[21,22] Thus, single melting point endotherms in the range of 171.1−174 °C, with no other endothermic transition, ruled out the possibility of experiencing in the current experimental setup the transformation of α Nif into β or γ forms.[22] Absence of solvate formation was assumed since no other solvent endothermic peak was observed in the DSC. These results were further supported by TGA thermographs (Figure 3), where no loss in weight was recorded until about 210 °C. Thus, from the results shown in Figures 2 and 3, the absence of any polymorphs and solvates was concluded.

3.4. FTIR and p-XRD Results of Selected Crystals. FTIR patterns of untreated Nif and all other crystallized formulation are shown in Figure 4. The spectra of all samples were identical, and the main absorption bands of Nif appeared in all the spectra. This indicated that all crystals displayed similar or no differences between the internal structure and conformation of these samples. Similarly the percent transmittance pattern shows the absence of any solvates. In p-XRD patterns as shown in Figure 5, characteristic peaks of Nif monoclinic form[20] were observed at 2θ values 7.5, 10.2, 11.3, 14.2, 16, 19.3, 22.2, and 24.8. These characteristic peaks were present in all other laboratory grown Nif crystals with slightly varying intensities. The reduction in intensity in a few crystals could be due to the higher crystal perfection or different preferred orientations of

dx.doi.org/10.1021/cg401612z | *Cryst. Growth Des.* 2014, 14, 326−338

the crystals in the sample holder, which may have occurred due to their different crystal habits. Therefore, the abundance of the planes exposed to the X-ray source would have been altered, producing the radiation in the relative intensities of the peak.[39] p-XRD patterns of all formulations were also compared with the simulated p-XRD pattern of the monoclinic form of Nif (CSD ref no. BICCIZ), which showed complete similarity and superimposable 2θ values ruling out the possibility of any other polymorphs of Nif. The reported characteristic p-XRD peaks of triclinic polymorphs of Nif were also not observed indicating that the samples are pure and consist with the monoclinic form.[21] Results from FTIR spectroscopy, X-ray analysis, and DSC taken together led to the conclusion that no polymorphs or solvates were formed and only habit modifications occurred during recrystallization of Nif under various conditions of crystallization.

3.5. Computational Study of Nif. Vacuum morphology was generated by the BFDH model, which gave eight important unique facets along with their planes (*hkl*), center to plane distance (d_{hkl}), and percent surface areas. Table 2 lists the interplanar spacings of various low index faces of the crystal habit of Nif based on the BFDH calculation. Results show that the crystal faces consist of (100), (011), (110), (002), (11$\bar{1}$), and (10$\bar{2}$) planes, of which (100) with 35.61% and (011) with 41.04% of total facial areas are the most important faces. However, the calculated aspect ratio of 1.83 was significantly different from the observed aspect ratio experimental habits in different solvents and antisolvents (Supporting Information).

Table 2. Surface Free Energies Calculated by the Morphology Growth Method and Attachment Energies Calculated by the Equilibrium Morphology Method

BFDH Model			
hkl	d_{hkl} (Å)	total facial area (Å^2)	surface area (%)
{100}	10.91	887.18	35.61
{011}	8.46	1022.31	41.04
{110}	7.49	184.14	7.39
{002}	7.39	339.36	13.62
{11$\bar{1}$}	6.77	27.08	1.087
{10$\bar{2}$}	6.26	30.84	1.23
Morphology Growth Model and Equilibrium Morphology Model			
hkl	d_{hkl} (Å)	E_{att} (kcal mol^{-1})	E_{sur} (kcal mol^{-1})	total facial area (Å^2)	surface area (%)
{100}	10.91	−22.50	28.22	7139.80	40.988
{011}	8.46	−31.47	27.69	7464.99	42.854
{110}	7.49	−38.72	37.47	338.34	1.942
{002}	7.39	−35.32	65.41	2476.07	14.214

In the second step, morphology was determined by the morphology growth model and equilibrium morphology model, which show all important faces with their *hkl*, d_{hkl}, surface areas, and surface energy values. The morphology growth model was used to calculate attachment energies of different faces, whereas the equilibrium model was used to calculate morphology at 0 K. Results in Table 2 show that the crystal faces consist of (100), (011), (110), and (002) planes, in which the (100) plane with 40.98% of the total facial area and the (011) plane with 42.85% of total facial area are the most important faces. The calculated aspect ratio for important selected faces was found to be 1.99 (Supporting Information), which was also observed as significantly different from the experimental habits. As discussed in previous sections, all models were initially simulated in vacuum. This significant deviation in the calculated values could be due to the absence of real conditions that were provided during crystallization experiments. Thus, there was a need to incorporate solvent molecules to predict habits that would be close to experimental habits. Few authors have successfully used this technique to predict the crystal habit with a fair degree of accuracy for drugs like haloperidol,[26] aspirin,[1] fenofibrate,[40] ginsenoside,[41] etc., while some authors reported limited correlation with simulated and experimentally grown crystals like ε-caprolactam,[42] 7-amino-4,6-dinitrobenzofurox-an,[36] etc. The possible reason for this unpredictability might be due to the major role played by underestimated electrostatic and van der Waals interactions.[43] This prediction method mostly assists solvent selection to improve the morphology in the drug crystallization process. For analyzing the impact of solvents and antisolvents on the crystal habits, a surface docking approach was used.[31]

As discussed in the crystallization section, on the basis of aspect ratio calculated during crystallization experiments supported with microscopic imaging data, five solvent combinations were selected for further studies. Under specific provided conditions of crystallization, the growth of one kind of crystal face may be retarded or another kind of face may be induced to grow faster.[44] It is suggested that polar solvents are preferentially adsorbed by polar faces and nonpolar solvents by nonpolar faces.[44] As a result, the polar surfaces are thought to be dominant when highly polar solvents are used while nonpolar surfaces are thought to be dominant when nonpolar solvents are used.[11] The relative abundance of polar and nonpolar moieties was studied on different faces of the Nif crystal habit obtained by attachment energy theory (Table 3 and Figure 6). In crystal slices, the (100) face shows an abundance of nonpolar carbon containing functional groups (four methyl groups) (Figure 6a), the (011) face shows an abundance of polar oxygen (one nitro and one carboxyl) and nitrogen (one amine) containing functional groups (Figure 6b), the (110) face shows an abundance of nonpolar carbon (two methyl groups) (Figure 6c), the (002) face shows an abundance of nonpolar carbon (two methyl and two aromatic rings) containing functional groups (Figure 6d), the (11$\bar{1}$) face shows an abundance of polar oxygen (two carboxyl) and nitrogen (two amine) containing functional groups (Figure 6e), the (111) face shows an abundance of nonpolar aliphatic (four methyl) and aromatic carbons (one aromatic ring) (Figure 6f), the (10$\bar{2}$) face shows an abundance of polar oxygen containing functional groups (two carboxyl and one nitro) (Figure 6g), and the (012) face shows an abundance of nonpolar carbon (two methyl and one aromatic ring) (Figure 6h). In next

Table 3. Surface Chemistry of the Dominant Crystal Faces (hkl) of Nifedipine

	number of functional group exposed to crystal surface				
hkl	CH_3	NH	NO_2	COO	aromatic ring
{100}	4			2	
{011}	2	1	1	1	1
{110}	2				
{002}	2		1	1	2
{11$\bar{1}$}	2	2		2	1
{111}	4	1		2	1
{10$\bar{2}$}	2		1	2	
{012}	2		1	1	1

dx.doi.org/10.1021/cg401612z | Cryst. Growth Des. 2014, 14, 326−338

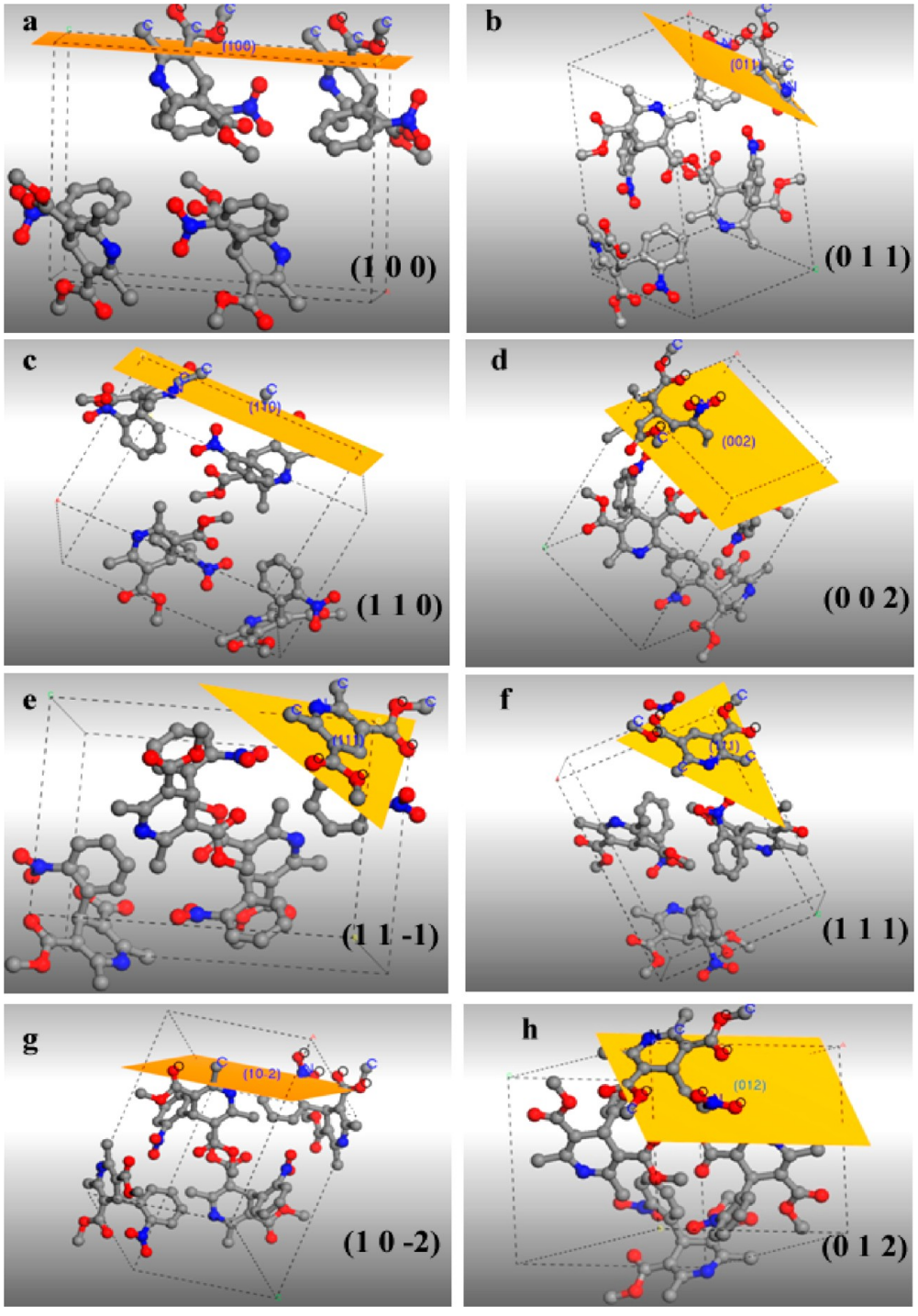

Figure 6. Crystal slices of different facets of Nif expressing the presence of polar and nonpolar functional groups.

section, the impact of selected solvents and their combinations on the surface morphology and possible interactions will be discussed.

3.5.1. Nif Morphology with Chloroform as Solvent and Hexane as Antisolvent. Isodiametric habit with an aspect ratio 1.357 ± 0.406 (n = 50) was obtained for Nif when chloroform was used as solvent and hexane was used as antisolvent (Figure 7a), while a rectangular habit with an aspect ratio 1.62 was predicted by computational method when provided with similar solvent conditions (Figure 7b). Statistically no significant difference was observed when aspect ratios of experimental and predicted habits were compared (p > 0.05), which was also confirmed by morphologically examination under a microscope (Figure 7a,b). The most prominent crystal faces were (100), (011), (111), (10$\bar{2}$), and (012) planes, in which the (011) contributed 35.05% of total facial area, the (100) plane contributed 22.23% of total facial area, and the (111) plane contributed 22.12% of total facial area (Table 4). The crystal face (011), due to the abundance of polar functional groups (one nitro, one carboxyl, and one amine), will dominate in a polar environment.[33] Similarly, the surface slices of (10$\bar{2}$) and (012) will also dominate in a polar environment due to the abundance of oxygen related polar functional groups. The surface slices of (100) and (111) however will dominate in a

dx.doi.org/10.1021/cg401612z | Cryst. Growth Des. 2014, 14, 326−338

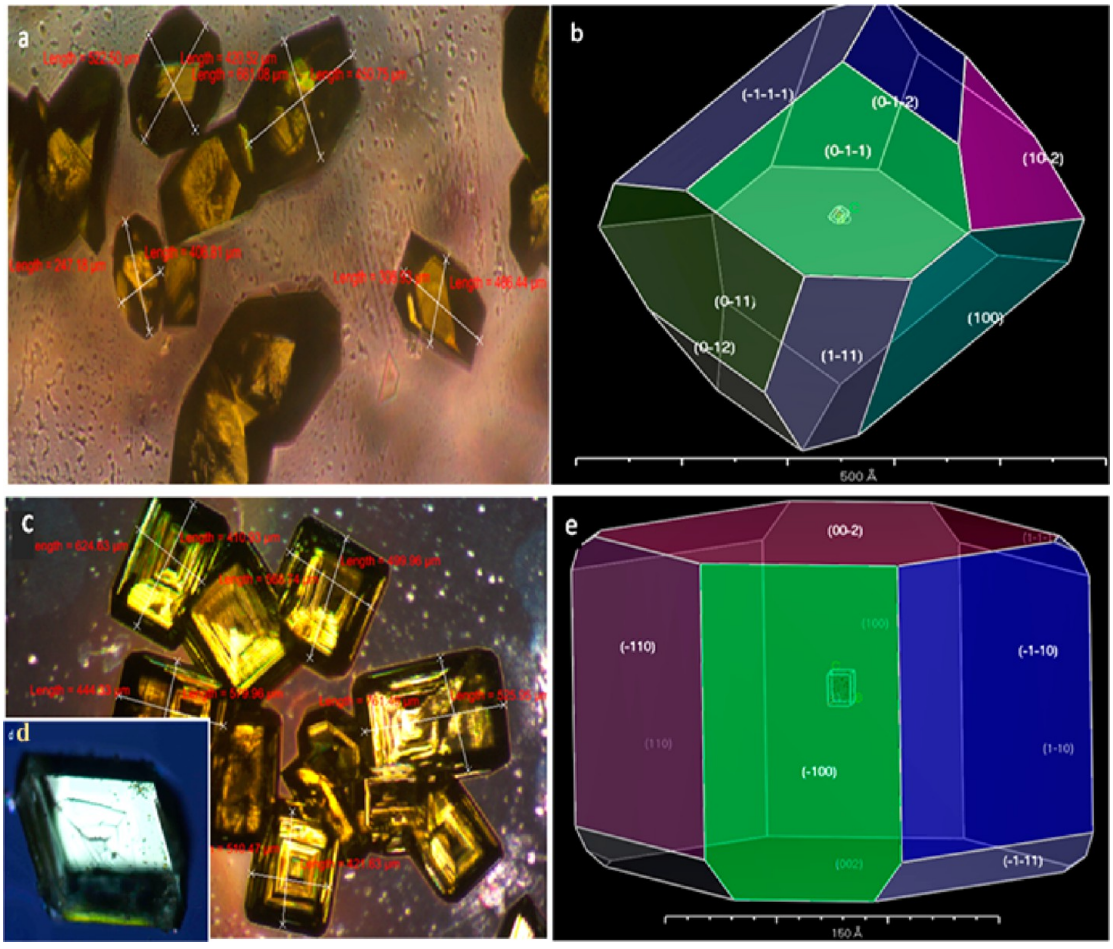

Figure 7. Modified crystal habits of Nif: (a) experimental habit with chloroform as solvent and hexane as antisolvent; (b) predicted habit with chloroform as solvent and hexane as antisolvent; (c) experimental habit 1 with chloroform as solvent and IPA as antisolvent; (d) experimental habit 2 with chloroform as solvent and IPA as antisolvent; (e) predicted habit with chloroform as solvent and IPA as antisolvent.

nonpolar environment due to the abundance of carbon related (methyl) nonpolar functional groups.[1] These Nif crystals showed about 57% of total facial area covered by polar functional groups and ~43% of total facial area covered by nonpolar functional moiety (Table 4). This proportional surface area can be correlated to proportion of crystallizing solvents, which included the weak polar solvent chloroform (75% v/v) and the nonpolar solvent hexane (25% v/v).

3.5.2. Nif Morphology with Chloroform as Solvent and IPA as Antisolvent. Cubical crystals with an aspect ratio of 1.338 ± 0.288 (n = 50) were obtained when Nif was recrystallized with chloroform as solvent and IPA as antisolvent (Figure 7c,d), whereas the predicted habit was also nearly isodiametric with aspect ratio of 1.74 (Figure 7e). Statistically there was no significant difference observed in experimental and predicted habits (p > 0.05), which was also confirmed by morphological examination under microscope (Figure 7c−e). Results in Table 4 show that the crystal faces consist of (100), (110), (002), (11$\bar{1}$), and (012) planes, in which (110) with 41.43% of total facial area, (002) with 32.35% of total facial area, and (100) with 19.61% of surface area are the most important faces. There exists an abundance of carbon related nonpolar functional groups, which can be clearly observed from surface slice of (110), (100), and (002) as shown in Figure 6a,c,d, respectively, indicating that these faces will dominate in a nonpolar environment. The abundance of oxygen related polar functional groups can be clearly observed from the surface slice of (11$\bar{1}$) shown in Figure 6e, which means that this face will dominate in a polar environment. On the basis of the results in Table 4, more than 80% of total facial area is covered by nonpolar functional groups and ~20% of total facial area is covered by polar functional moieties. This proportional surface area can be correlated to the proportion of crystallizing solvents, which comprised a comparatively weak polar solvent chloroform (75% v/v) and polar solvent IPA (25% v/v).

3.5.3. Nif Morphology with DCM as Solvent. Cubical crystals with an aspect ratio of 1.32 ± 0.264 (n = 50) were obtained when Nif was recrystallized with DCM as solvent (Figure 8a,b), while the predicted habit was also nearly cubic with an aspect ratio of 1.846 (Figure 8c). Statistically, no significant difference was observed in experimental and predicted habits (p > 0.05), which was also confirmed by morphological examination under microscope (Figure 8a−c). Results in Table 4 show that the crystal faces consist of (002), (111), (10$\bar{2}$), and (012) planes, of which the (111) with 50.33% of total facial area, the (012) with 21.35% of total facial area, and the (10$\bar{2}$) with 17.34% of total facial area are the most important faces. The abundance of carbon related aromatic and aliphatic nonpolar functional groups can be clearly observed from the surface slices of (002), (111), and (012) shown in Figure 6d,f,h, respectively, which means that these faces will dominate in a nonpolar environment, while the surface slice of

dx.doi.org/10.1021/cg401612z | Cryst. Growth Des. 2014, 14, 326−338

Table 4. Modified Attachment Energies, Percentage of Facet Area, Total Surface Area, Volume, and Surface/Volume (S/V) of Nif Grown in Solvents and Solvent−Antisolvent Combinations, Calculated by Surface Docking Approach

solvent/antisolvent	*hkl*	$^{mod}E_{att}$ (kcal mol^{-1})	total facial area (Å^2)	% total facial area	total surface area (Å^2)	volume (Å^3)	*S*/*V*
Nif−chloroform/hexane	{100}	−154.10	109707	22.23	473381.3	27526550	1.110
	{011}	−161.59	172967	35.05			
	{111}	−172.76	109154	22.12			
	{10$\bar{2}$}	−187.08	51951	10.52			
	{012}	−184.42	49600	10.05			
Nif−chloroform/IPA	{100}	−77.50	28012.03	19.61	142845.5	3971907	1.178
	{110}	−85.91	59192.36	41.43			
	{002}	−79.19	46218.57	32.35			
	{11$\bar{1}$}	−105.36	9084.60	6.35			
	{012}	−125.40	337.89	0.23			
Nif−DCM	{002}	−29.22	2206	10.95	653880.6	42274470	1.114
	{111}	−31.30	10134.08	50.33			
	{10$\bar{2}$}	−33.10	3492.20	17.34			
	{012}	−32.46	4299.38	21.35			
Nif−DCM/IPA	{100}	78.35	1799.86	3.19	56382.51	1034673	1.140
	{11$\bar{1}$}	−63.78	6738.32	11.95			
	{111}	−61.85	14700.22	26.07			
	{10$\bar{2}$}	−48.29	9884.74	17.53			
	{012}	−49.30	23259.36	41.25			
Nif−ethanol/hexane	{011}	−179.90	213154.3	32.59	643880.6	42274470	1.104
	{110}	−200.84	196974	30.12			
	{002}	−204.18	61419.75	9.39			
	{111}	−225.19	69984.86	10.70			
	{10$\bar{2}$}	−183.50	112347.7	17.18			

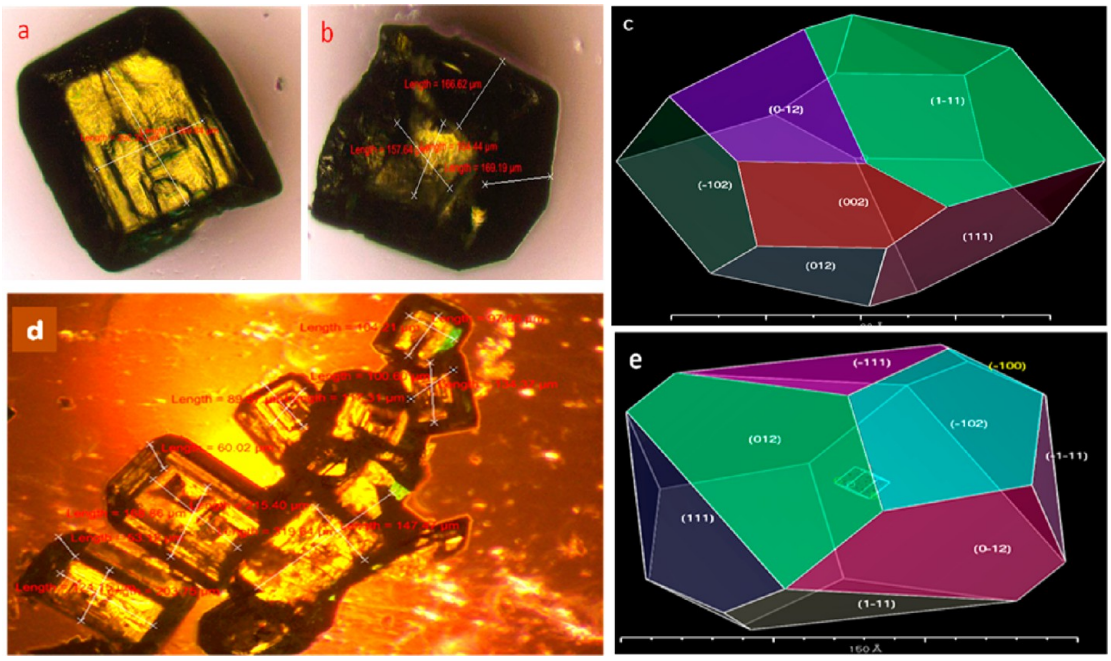

Figure 8. Modified crystal habits of Nif: (a) experimental habit 1 with DCM as solvent; (b) experimental habit 2 with DCM as solvent; (c) predicted habit with DCM as solvent; (d) experimental habit with DCM as solvent and IPA as antisolvent; (e) predicted habit with DCM as solvent and IPA as antisolvent.

(10$\bar{2}$) due to the abundance of oxygen related polar functional groups will dominate in a polar environment. Approximately 70% of total facial area is covered by nonpolar functional groups, and ∼30% of total facial area is covered by polar functional moieties (Table 4). This proportional surface area can be correlated to the polarity index of the crystallizing solvent DCM, which lies at the bottom of polar aprotic solvents with weak hydrogen bond formation capacity. DCM is aprotic with weak H-bonding capacity and hence will not affect crystal growth according to any specific surface functionality, unlike polar or nonpolar solvents. This nature will give nearly isodiametric crystals, which can be clearly seen in Figure 8a−c.

3.5.4. Nif Morphology with DCM as Solvent and IPA as Antisolvent. Nearly cubical crystals with aspect ratio of 1.41 ±

dx.doi.org/10.1021/cg401612z | *Cryst. Growth Des.* 2014, 14, 326−338

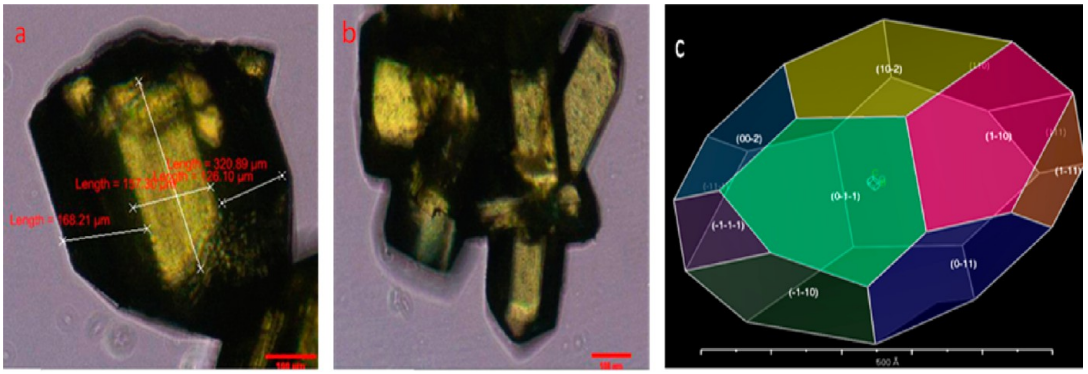

Figure 9. Modified crystal habits of Nif with ethanol as solvent and hexane as antisolvent: (a) experimental habit 1; (b) experimental habit 2; (c) predicted habit.

0.30 (n = 50) were obtained when Nif was recrystallized with DCM as solvent and IPA as antisolvent (Figure 8d), while the predicted habit as shown in Figure 8e was also nearly isodiametric with an aspect ratio of 1.77, which was statistically insignificant (p > 0.05) to the predicted values. The morphological similarity between experimental and predicted habits can also be clearly observed from Figure 8d,e. The predicted crystal faces consisted of (100), (11$\bar{1}$), (111), (10$\bar{2}$), and (012) planes, of which the (012) with 41.25% of total facial area and the (111) with 26.07% of total facial area are the most important faces (Table 4). The abundance of oxygen related polar functional groups from the surface slices of (11$\bar{1}$), (10$\bar{2}$), and (012) as shown in Figure 6e,g,h, respectively, indicate that these faces will dominate in a polar environment. The subtle presence of nonpolar aromatic carbon groups that are also visible from the surface slice of (012) means that this face will also support growth in a nonpolar environment to some extent. From the surface slices of (100) and (111) shown in Figure 6a,f, the abundance of carbon related nonpolar functional groups can be clearly observed, which means that these faces will dominate in a nonpolar environment. In conclusion, 70% of total facial area of the crystal developed from DCM and IPA is covered by polar functional groups, and ∼30% of total facial area is covered by nonpolar functional moieties (Table 4), which could be correlated to the proportion of crystallizing solvents that include aprotic weak polar solvent DCM (75% v/v) and polar solvent IPA (25% v/v).

3.5.5. Nif Morphology with Ethanol as Solvent and Hexane as Antisolvent. Isodiametric (∼spherical) crystals with an aspect ratio of 1.459 ± 0.194 (n = 50) were obtained when Nif was recrystallized with ethanol as solvent and hexane as antisolvent (Figure 9a,b), whereas the predicted habit in same solvent system was also ∼spherical with aspect ratio of 1.70 (Figure 9c). Statistically no significant difference was observed in experimental and predicted habits (p > 0.05), which was also confirmed by morphological examination under a microscope (Figure 9a−c). Results in Table 4 show that the crystal faces consist of (011), (110), (002), (111), and (10$\bar{2}$) planes, of which the (011) with 32.59% of total facial area and the (110) with 30.12% of total facial area are the most important faces. The abundance of oxygen related polar functional groups can be clearly observed from the surface slices of (011) and (10$\bar{2}$), as shown in Figure 6b,g, respectively, which means that these faces will dominate in a polar environment. The abundance of carbon related nonpolar functional groups followed by the subtle presence of polar oxygen groups can be clearly observed from the surface slice of (110) shown in Figure 6c, which means that this face will dominate in a nonpolar environment followed by a polar one, while the abundance of carbon related nonpolar functional groups on (002) and (111) shown in Figure 6d,f indicates that these faces will dominate in a nonpolar environment. On the basis of results shown in Table 4, we can observe that 50−60% of total facial area is covered by polar functional groups and 40−50% of total facial area is covered by nonpolar functional moieties (Table 4), which can be correlated to the proportion of crystallizing solvents, which consisted of polar solvent ethanol (75% v/v) and nonpolar solvent hexane (25% v/v).

3.6. Comparison of Predicted Solvent-Mediated Morphology with Experimental Morphology. The solvent-mediated MAE calculations based on the scaling of the basic attachment energy data using the molecular dynamics calculations predict the solution growth morphology of Nif with differing degrees of success. In the case of Nif, the habit modification is caused by surface−solvent interactions, which affect the growth rate of the polar and nonpolar faces differently (Figure 6). There exists a significant similarity (p < 0.05) between experimental and predicted crystal habits of all five selected combinations (Figure 10). From the results of experimental habits, it was demonstrated that nearly isodiametric and comparatively best crystals were obtained when Nif was recrystallized with chloroform/IPA and DCM/IPA as solvent/antisolvent pairs.

3.7. Comparative Solubility and Dissolution Rate. A significant improvement (p < 0.05) in equilibrium solubility of

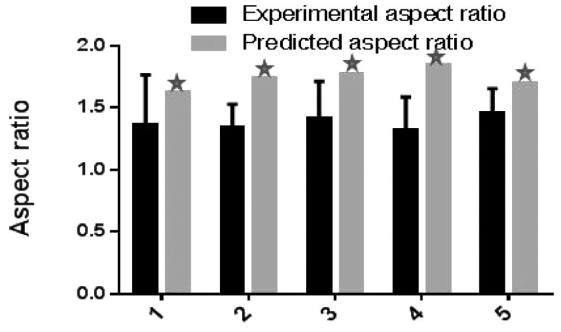

Figure 10. Correlation between experimental aspect ratio and predicted aspect ratio: (1) Nif with chloroform and hexane; (2) Nif with chloroform and IPA; (3) Nif with DCM; (4) Nif with DCM and IPA; (5) Nif with ethanol and hexane; ★ indicates insignificant difference between predicted aspect ratio and experimental aspect ratio (p > 0.05).

dx.doi.org/10.1021/cg401612z | *Cryst. Growth Des.* 2014, 14, 326−338

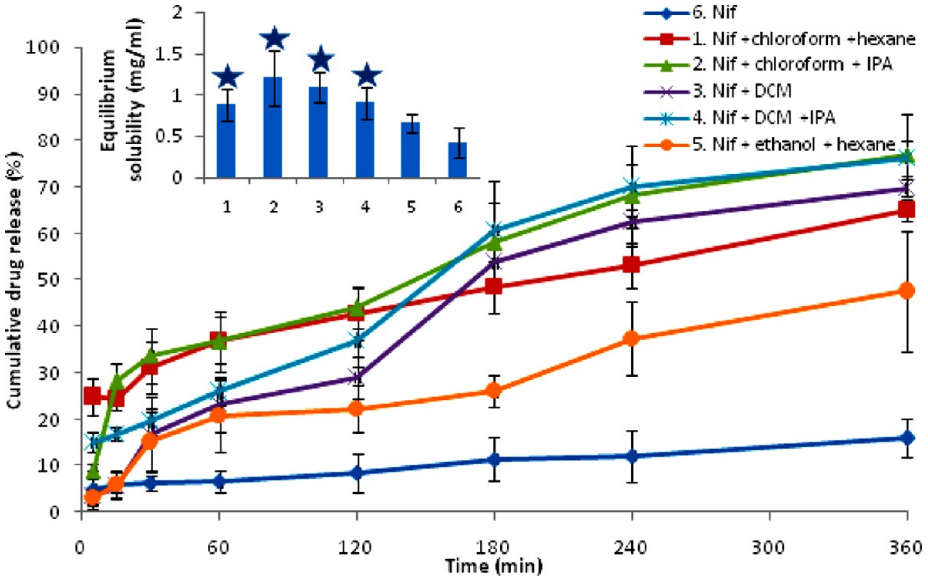

Figure 11. Comparative dissolution profile of different Nif formulations. Inset shows comparative equilibrium solubility profile of different Nif formulations; ★ indicates significant difference in equilibrium solubility when compared with 6 ($p < 0.05$).

four different crystal habits was observed compared with plain Nif (Figure 11). Nif when crystallized with chloroform as solvent and IPA as antisolvent showed maximum solubility (1.29 ± 0.34 mg/mL) compared with other crystallizing systems, chloroform/hexane, DCM, and DCM/IPA, and untreated Nif (0.43 ± 0.19 mg/mL). This marked improvement could be attributed to the isometric morphology of the crystals grown in chloroform and IPA system. Nif when crystallized from the ethanol/hexane system also showed improvement in equilibrium solubility (0.66 ± 0.12 mg/mL), but this was found to be statistically insignificant ($p > 0.05$) compared with untreated Nif.

Crystal habit modification resulted in significant dissolution improvement (Figure 11). Nif with chloroform as solvent and IPA as antisolvent, Nif with DCM, and Nif with DCM as solvent and IPA as antisolvent showed significant improvement in dissolution rate. Nif with chloroform as solvent and hexane as antisolvent and Nif with ethanol as solvent and hexane as antisolvent also showed improvement in dissolution rate but not to the extent shown by previous combinations. The order of dissolution rate was 2 > 4 > 3 > 1 > 5. The difference in dissolution rate is often related to the surface area of various crystals with different shapes (volume). Because of the structural variation, the orientation of molecules on the surface of each facet of a crystal is different. The different relative abundance of crystal facets between crystal habits will lead to different surface properties. We hypothesized that these differences resulted from different relative abundance of various facets in the two crystal habits. As shown in Table 4, surface area (S)/volume (V) ratio of these simulated habits were found to be in the order 2 > 4 > 3 > 1 > 5, which correlates well with the dissolution rate. This level of improvement is relevant to biopharmaceutical performance of drugs with poor solubility.

4. CONCLUSION

The crystal morphology of Nif was studied by molecular simulation. The preliminary results obtained from classical methods have provided some basic information about the morphology; however, they were found to be significantly different from the experimental habit. By introduction of the surface docking approach, the simulation results were found to be significantly closer to the observed habit. This model could depict the solvent effect on crystal morphology with a fair degree of accuracy and was found to be closer to the actual situation than the other models. It is also reasonable to believe that this model can be applied to other drug molecules to study the relationship among crystal morphology and solvation effects.

■ ASSOCIATED CONTENT

Supporting Information

BFDH morphology, morphology growth model, individual p-XRD of Nif and selected combinations, simulated p-XRD of α polymorph of Nif and simulated p-XRD of β polymorph of Nif. This material is available free of charge via the Internet at http://pubs.acs.org.

■ AUTHOR INFORMATION

Corresponding Author

*Tel: +91-08125849395. Fax: +91-040-23073751. E-mail: svcphod@yahoo.co.in, nalini@niperhyd.ac.in.

Notes

The authors declare no competing financial interest.

■ ACKNOWLEDGMENTS

The authors acknowledge Dr. G. Desiraju (Indian Institute of Science Bangalor, India) and Dr. Ashwini Nangia (Hyderabad Central University, India) for scientific inspiration. Authors also acknowledge financial support from the National Institute of Pharmaceutical Education & Research (NIPER), Hyderabad, India, and Indian Institute of Chemical Technology (IICT), Hyderabad, India.

■ ABBREVIATIONS

DCM, dichloromethane; IPA, isopropyl alcohol; MD, molecular dynamics; Nif, nifedipine; BFDH, Bravais–Friedel–Donnay–Harkel; DSC, differential scanning calorimetry;

TGA, thermogravimetric analysis; FTIR, Fourier transform infrared; p-XRD, powder X-ray diffraction

REFERENCES

(1) Li, T.; Li, B.; Tomassone, M. S. *Chem. Eng. Sci.* **2006**, *61* (15), 5159−5169.
(2) Hartman, P. *Physics and Chemistry of the Organic Solid State*; Fox, D., Labes, M. M., Weissberger, A., Eds.; Interscience: New York. 1963.
(3) Mirza, S.; Miroshnyk, I.; HeinaÌmaÌki, J.; Rantanen, J.; Antikainen, O.; Vuorela, P.; Vuorela, H.; Yliruusi, J. *Cryst. Growth Des.* **2008**, *8* (10), 3526−3531.
(4) Haleblian, J. K. *J. Pharm. Sci.* **1975**, *64* (8), 1269−1288.
(5) Kopp, S.; Beyer, C.; Graf, E.; Kubel, F.; Doelker, E. *J. Pharm. Pharmacol.* **1989**, *41* (2), 79−82.
(6) Variankaval, N.; Cote, A. S.; Doherty, M. F. *AIChE J.* **2008**, *54* (7), 1682−1688.
(7) Doherty, C.; York, P. *Int. J. Pharm.* **1988**, *47* (3), 141−155.
(8) York, P. *Drug Dev. Ind. Pharm.* **1992**, *18* (6−7), 677−721.
(9) Kuvadia, Z. B.; Doherty, M. F. *Cryst. Growth Des.* **2013**, *13* (4), 1412−1428.
(10) Iohara, D.; Yoshida, K.; Yamaguchi, K.; Anraku, M.; Motoyama, K.; Arima, H.; Uekama, K.; Hirayama, F. *Cryst. Growth Des.* **2012**, *12* (4), 1985−1991.
(11) Shariare, M. H.; Blagden, N.; Matas, M. d.; Leusen, F. J. J.; York, P. *J. Pharm. Sci.* **2011**, *101* (3), 1108−1119.
(12) Blagden, N.; De Matas, M.; Gavan, P.; York, P. *Adv. Drug Delivery Rev.* **2007**, *59* (7), 617−630.
(13) Erk, P.; Hengelsberg, H.; Haddow, M. F.; van Gelder, R. *CrystEngComm* **2004**, *6* (78), 474−483.
(14) Yani, Y.; Chow, P. S.; Tan, R. B. H. *Mol. Pharmaceutics* **2011**, *8* (5), 1910−1918.
(15) Dey, A.; Kirchner, M. T.; Vangala, V. R.; Desiraju, G. R.; Mondal, R.; Howard, J. A. K. *J. Am. Chem. Soc.* **2005**, *127* (30), 10545−10559.
(16) Schmidt, C.; Ulrich, J. *J. Cryst. Growth.* **2012**, *353* (1), 168−173.
(17) Blagden, N. *Powder Technol.* **2001**, *121* (1), 46−52.
(18) Braunwald, E. *New Engl. J. Med.* **1982**, *307* (26), 1618.
(19) Devarakonda, B.; Hill, R. A.; de Villiers, M. M. *Int. J. Pharm.* **2004**, *284* (1), 133−140.
(20) Klimakow, M.; Rademann, K.; Emmerling, F. *Cryst. Growth Des.* **2010**, *10* (6), 2693−2698.
(21) Gunn, E.; Guzei, I. A.; Cai, T.; Yu, L. *Cryst. Growth Des.* **2012**, *12* (4), 2037−2043.
(22) Grooff, D.; De Villiers, M. M.; Liebenberg, W. *Thermochim. Acta* **2007**, *454* (1), 33−42.
(23) Hecq, J. r. m.; Deleers, M.; Fanara, D.; Vranckx, H.; Amighi, K. *Int. J. Pharm.* **2005**, *299* (1), 167−177.
(24) Destri, G. L.; Marrazzo, A.; Rescifina, A.; Punzo, F. *J. Pharm. Sci.* **2013**, *102* (1), 73−83.
(25) Punzo, F. *J. Mol. Struct.* **2013**, *1031*, 147−154.
(26) Destri, G. L.; Marrazzo, A.; Rescifina, A.; Punzo, F. *J. Pharm. Sci.* **2011**, *100* (11), 4896−4906.
(27) Yang, W.; de Villiers, M. M. *Eur. J. Pharm. Biopharm.* **2004**, *58* (3), 629−636.
(28) Qureshi, S. A.; Caille, G.; Brien, R.; Piccirilli, G.; Yu, V.; McGilveray, I. J. *Drug Dev. Ind. Pharm.* **1994**, *20* (11), 1869−1882.
(29) Schmidt, C.; Ulrich, J. *Chem. Eng. Technol.* **2012**, *35* (6), 1009−1012.
(30) Chen, J.; Trout, B. L. *Cryst. Growth Des.* **2010**, *10* (10), 4379−4388.
(31) Lu, J. J.; Ulrich, J. *Cryst. Res. Technol.* **2003**, *38* (1), 63−73.
(32) Yang, L.; Dong, Y. *Carbohydr. Res.* **2011**, *346* (15), 2457−2462.
(33) Kiang, Y. H.; Yang, C.-Y.; Staples, R. J.; Jona, J. *Int. J. Pharm.* **2009**, *368* (1), 76−82.
(34) Lemmer, S.; Ruether, F. *Chem. Eng. Sci.* **2011**, *77*, 143−149.
(35) Zhou, K.; Li, J.; Luo, J.; Jin, Y. *Chin. J. Chem. Eng.* **2012**, *20* (3), 602−607.
(36) Lee, H.-E.; Lee, T. B.; Kim, H.-S.; Koo, K.-K. *Cryst. Growth Des.* **2010**, *10* (2), 618−625.
(37) Eckert, T.; Miller, J. *Arch. Pharm.* **1977**, *310* (2), 116−118.
(38) Burger, A.; Koller, K. T. *Sci. Pharm.* **1996**, *64* (3−4), 293−301.
(39) Marshall, P. V.; York, P. *Int. J. Pharm.* **1989**, *55* (2), 257−263.
(40) Zhu, W.; Romanski, F. S.; Meng, X.; Mitra, S.; Tomassone, M. S. *Eur. J. Pharm. Sci.* **2011**, *42* (5), 452−461.
(41) Gu, H.; Li, R.; Sun, Y.; Li, S.; Dong, W.; Gong, J. *J. Cryst. Growth.* **2012**, *373*, 146−150.
(42) Walker, E. M.; Roberts, K. J.; Maginn, S. J. *Langmuir* **1998**, *14* (19), 5620−5630.
(43) Stoica, C.; Verwer, P.; Meekes, H.; Van Hoof, P.; Kaspersen, F. M.; Vlieg, E. *Cryst. Growth Des.* **2004**, *4* (4), 765−768.
(44) Nokhodchi, A.; Bolourtchian, N.; Dinarvand, R. *Int. J. Pharm.* **2003**, *250* (1), 85−97.